

Finite element modeling of concentric-tube continuum robots

Changyeob Baek¹, Kyungho Yoon² and Do-Nyun Kim^{*1,2}

¹Department of Mechanical and Aerospace Engineering, Seoul National University,
Gwanak-ro 1, Gwanak-gu, Seoul 08826, Republic of Korea

²Institute of Advanced Machines and Design, Seoul National University,
Gwanak-ro 1, Gwanak-gu, Seoul 08826, Republic of Korea

(Received September 2, 2015, Revised November 30, 2015, Accepted December 14, 2015)

Abstract. Concentric-tube continuum robots have formed an active field of research in robotics because of their manipulative exquisiteness essential to facilitate delicate surgical procedures. A set of concentric tubes with designed initial curvatures comprises a robot whose workspace can be controlled by relative translations and rotations of the tubes. Kinematic models have been widely used to predict the movement of the robot, but they are incapable of describing its time-dependent hysteretic behaviors accurately particularly when snapping occurs. To overcome this limitation, here we present a finite element modeling approach to investigating the dynamics of concentric-tube continuum robots. In our model, each tube is discretized using MITC shell elements and its transient responses are computed implicitly using the Bathe time integration method. Inter-tube contacts, the key actuation mechanism of this robot, are modeled using the constraint function method with contact damping to capture the hysteresis in robot trajectories. Performance of the proposed method is demonstrated by analyzing three specifications of two-tube robots including the one exhibiting snapping phenomena while the method can be applied to multiple-tube robots as well.

Keywords: concentric-tube continuum robot; finite element; hysteresis; contact

1. Introduction

Several research groups have recently proposed novel continuum robot designs (Fig. 1) consisting of several concentric tubes (Dupont *et al.* 2009, Dupont *et al.* 2010, Rucker *et al.* 2010, Webster *et al.* 2006, Webster *et al.* 2009, Sears and Dupont 2006). Unlike conventional robots composed of discrete joints and links, these robots produce various motions using the flexibility of continuous structures and only a small number of actuators attached to its base. Manipulating its basal end leading to successive translations and rotations of comprising tubes can control the distal end of the robot, which is usually equipped with an end-effector such as a gripper, a surgical knife, or a needle. This simple actuating mechanism miniaturizes the structure of the robot with typical tube diameters of several millimeters, which renders its potential usage effective in medical applications, mainly in minimally invasive surgery, such as tumor removal (Burgner *et al.* 2011), intracerebral hemorrhage evacuation (Burgner *et al.* 2013), and transnasal surgery (Burgner *et al.* 2014).

*Corresponding author, Assistant Professor, E-mail: dnkim@snu.ac.kr

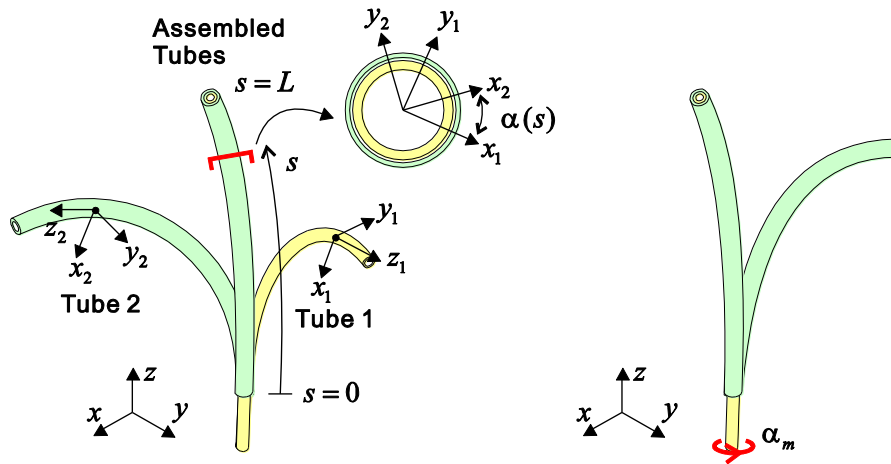


Fig. 1 Concentric-tube continuum robot

Analysis and design of these tube robots have been mostly done using the kinematics-based modeling approaches so far. Dupont *et al.* and Webster *et al.* concurrently and independently derived the second order nonlinear differential equations with consideration for the flexural and torsional energies of the tubes using the Cosserat rod theory and provided the analytic solution for two-tube continuum robots (Dupont *et al.* 2009, Dupont *et al.* 2010, Rucker *et al.* 2010, Webster *et al.* 2009). Due to the simplicity of the kinematic model, it provides quickly the trajectory of the robot as a function of base inputs for a given tube specification. In particular, it can predict a snapping phenomenon that occurs when the highly curved tubes overlapped over a long region are used. At the moment of snapping, the distal end of the robot rotates abruptly and considerably with respect to the input at its base, which would be extremely dangerous in surgical operations.

However, the kinematic model neglects several important geometric and mechanical factors including the gap, surface friction and contact damping between the tubes. For example, the kinematic model assumes zero clearance between the tubes suggesting that every tube has the same curvature over the entire region of overlap in equilibrium, which is not valid in reality. It has been reported that the experimental trajectories deviate from the trajectories obtained using the kinematic model although it is not clear which factors excluded from the model are responsible for the observed errors (Dupont *et al.* 2010). In particular, the kinematic model is unable to predict the time-dependent hysteretic motion of the robot at all. Tube robots can have multiple states of configuration depending on the input sequence at the basal end, but the kinematic model can predict a single state only regardless of input history (Dupont *et al.* 2009, Dupont *et al.* 2010).

To overcome this limitation, we present in this paper a finite element analysis framework for concentric-tube continuum robots. Dynamic motions of the robot in response to the applied base inputs are calculated implicitly using the Bathe time integration method (Bathe and Baig 2005, Bathe 2007, Bathe and Noh 2012, Noh *et al.* 2013) where the tubes are triangulated using the MITC shell elements (Kim and Bathe 2008, Kim and Bathe 2009, Lee and Bathe 2004, Lee *et al.* 2012). Contact-based interactions between the tubes are modeled using the constraint function method (Bathe and Bouzinov 1997). Here we incorporate the isotropic viscous damping effect into the interaction model assuming energy dissipation while the tubes are in contact with each other, which is essential to capture the time-dependent hysteretic behaviors of the robot.

This paper is organized as follows. First, a brief introduction to the kinematic model is given in section 2 and then the proposed finite element modeling approach is discussed in section 3. Section 4 demonstrates the performance of the proposed model for concentric-tube continuum robots by analyzing two-tube robots with three types of tube specifications including the one shows the unstable snapping phenomenon. Finally, we conclude with summary in section 5.

2. Kinematic model

In this section, we briefly review the kinematic model for concentric-tube continuum robots developed concurrently but independently by Dupont *et al.* and Webster *et al.* using the Cosserat rod theory (Dupont *et al.* 2010, Rucker *et al.* 2010). For simplicity, we focus on the kinematics of two-tube robots with the following conditions: (1) each tube has a piecewise constant curvature, (2) two tubes are aligned initially on a plane and (3) only rotational base inputs are applied.

We first define the time-dependent curvature vectors of each tube as a function of the arc length (s) measured from the base position of the outer tube as

$$\mathbf{u}_i(s)^T = [u_{ix}(s) \quad u_{iy}(s) \quad u_{iz}(s)] \quad (1)$$

and their initial curvature before applying base inputs

$$\hat{\mathbf{u}}_i(s)^T = [\hat{u}_{ix}(s) \quad \hat{u}_{iy}(s) \quad \hat{u}_{iz}(s)] \quad (2)$$

where i represents the tube index ($i=1$ for the outer tube and $i=2$ for the inner tube) and x , y and z denote the axes of each tube's material frame (Fig. 1). Then, the three-dimensional motion of the two-tube robot can be described by a set of differential equations

$$\mathbf{u}_2(s)|_{x,y} = (\mathbf{K}_1 + \mathbf{K}_2)_{x,y}^{-1} (\mathbf{R}_z^T(\alpha(s))\mathbf{K}_1\hat{\mathbf{u}}_1(s) + \mathbf{K}_2\hat{\mathbf{u}}_2(s))_{x,y} \quad (3)$$

$$\dot{\alpha} = (1 + k_{2z}/k_{1z})u_{2z} \quad (4)$$

$$\dot{u}_{2z} = (k_{2x}/k_{2z})(u_{2x}\hat{u}_{2y} - u_{2y}\hat{u}_{2x}) \quad (5)$$

where $\alpha(s) = \theta_2(s) - \theta_1(s)$ is the relative twist angle between the two tubes, $\mathbf{R}_z(\alpha)$ is the rotation matrix corresponding to rotation by α about z -axis and the dot represents the derivative with respect to s . \mathbf{K}_i is the stiffness matrix of tube i defined as

$$\mathbf{K}_i = \begin{bmatrix} k_{ix} & 0 & 0 \\ 0 & k_{iy} & 0 \\ 0 & 0 & k_{iz} \end{bmatrix} = \begin{bmatrix} E_i I_i & 0 & 0 \\ 0 & E_i I_i & 0 \\ 0 & 0 & G_i J_i \end{bmatrix} \quad (6)$$

where E_i is the Young's modulus, I_i is the area moment of inertia, J_i is the polar moment of inertia and G_i is the shear modulus with z -axis tangential to the resultant centerline of the robot. We can obtain $\mathbf{u}_i(s)$ and $\alpha(s)$ by solving Eqs. (3)-(5) simultaneously using conventional numerical algorithms for ordinary differential equations.

Alternatively, if we assume that tube curvatures are piecewise constant, we can derive a single second-order differential equation for $\alpha(s)$

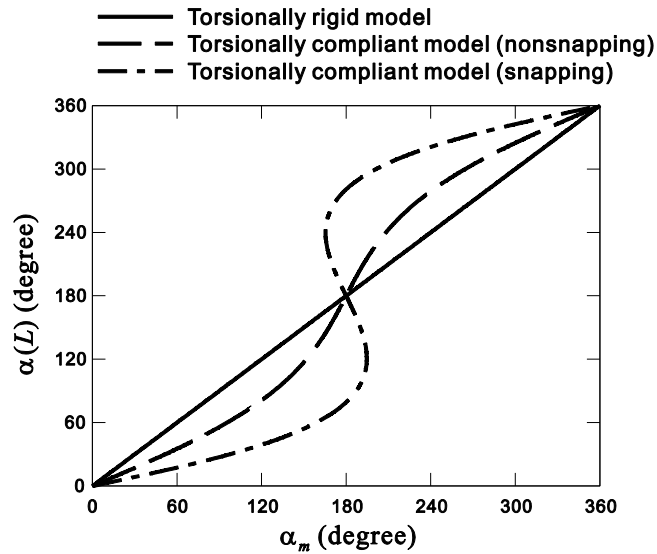


Fig. 2 Relative twist angle curves calculated using the kinematic models

$$\ddot{\alpha}(s) = (1 + \nu)\kappa_1(s)\kappa_2(s)\sin \alpha(s) = c(s)\sin \alpha(s) \quad (0 \leq s \leq L) \quad (7)$$

where ν is Poisson's ratio, and $\kappa_1(s)$ and $\kappa_2(s)$ are piecewise constant curvatures and L is the arc length of the overlapped region. When $c(s)$ is constant, Eq. (7) reduces to the governing equation of the inverted pendulum whose analytic solution is available (Dupont *et al.* 2010, Rucker *et al.* 2010). Hence, we can calculate $\alpha(s)$ first by solving Eq. (7) and then obtain $\mathbf{u}_i(s)$ by simply substituting $\alpha(s)$ into Eqs. (3)-(4). Once we obtain the curvature vectors of the tubes at every point along the tube, we can easily trace back the centerline positions of the robot using conventional operations of matrix exponents (Rucker *et al.* 2010).

In order to solve Eq. (7), two boundary conditions are necessary. The first boundary condition comes from the input twist angles at the basal end, $\theta_1(0)$ and $\theta_2(0)$, that can be controlled manually or automatically by a motor system leading to

$$\alpha(0) = \theta_2(0) - \theta_1(0) \quad (8)$$

Moment-free condition at the distal end provides the second boundary condition that can be written as

$$\dot{\alpha}(L) = 0 \quad (9)$$

In general, the relative twist angle at the distal end, $\alpha(L)$, can be measured experimentally and plotted with respect to the basal input angle $\alpha(0) \in [0, 2\pi]$. This twist angle curve is then used to evaluate the accuracy of the kinematic models, which is closely related to the tube curvatures and consequently to the robot trajectories (Dupont *et al.* 2009, Dupont *et al.* 2010). If the tubes were rigid in torsion, the twist angle curve would be a straight line regardless of tube specification, however, the real curves are S-shaped due to the torsional compliance of tubes (Fig. 2). It is noteworthy that unstable snapping phenomena of the robot occur when the tubes are highly curved initially and their overlapped region is long, which has been reported and verified both

theoretically and experimentally (Dupont *et al.* 2009, Dupont *et al.* 2010, Rucker *et al.* 2010, Webster *et al.* 2009). The kinematic model can predict these features of the twist angle curve successfully.

One major drawback of the kinematic model is the fact that it provides a single curve only for the relative twist angle at the distal end although it has been observed experimentally that the robot can have two different output angles for the same input angle depending on the direction of rotation (Dupont *et al.* 2009, Dupont *et al.* 2010). As a result, there exist two curves corresponding to the clockwise (CW) and counterclockwise (CCW) rotations that form a closed, hysteresis loop. It has been pointed out that the error in the tip position predicted by the kinematic model can be up to ten percent of the total length of the robot because of this hysteretic behavior of the robot (Lock and Dupont 2011), which amounts to a few centimeters for a typical surgical robot that can be critical in delicate surgical procedures.

3. Finite element model

To overcome the limitation of the kinematic model, we develop a finite element model for concentric-tube continuum robots. Robust numerical methods for highly nonlinear dynamic analysis of thin shell structures must be employed to obtain a reliable solution for the robot because it consists of multiple thin-walled tubes with initial curvature, utilizes the contact force between the tubes to transmit actuating basal input to the distal end and undergoes large displacements with hysteresis. Here, we establish a systematic analysis procedure to predict robot trajectories using a commercial finite element analysis program ADINA (ADINA R&D 2013) that provides the necessary modeling capabilities. Transient responses of the robot are computed implicitly using the Bathe method (Bathe and Baig 2005, Bathe 2007, Bathe and Noh 2012, Noh *et al.* 2013) where the tubes are modeled using the MITC shell elements (Lee and Bathe 2004, Kim and Bathe 2008, Kim and Bathe 2009, Lee *et al.* 2012) and contact conditions between them are imposed via the constraint function method (Bathe and Bouzinov 1997) assuming isotropic contact damping. The procedure largely consists of two consecutive analysis steps: (1) tube assembly step where the finite element models of individual tubes with various curvatures are constructed and assembled into the equilibrium configuration and (2) robot actuation step where the tube trajectories are computed dynamically in response to actuation inputs at the base position. To illustrate, we consider two-tube robots only in this study while the proposed procedure can be applied to robots consisting of multiple tubes as well.

3.1 Tube assembly

First of all, we need to construct a computational model for the robot comprising initially curved tubes. A naive approach to generating the tube assembly would be to build individual tube models first and then integrate them successively by inserting a smaller tube into a larger one from one end to the other end. However, this approach usually suffers from an issue of slow or no convergence particularly when assembling tubes with different curvature. This difficulty stems mainly from the fact that multiple contacts occur between the tubes and their locations keep changing during analysis making contactor nodes oscillate between several target nodes without convergence in certain cases. To resolve this problem, we develop another approach that can assemble the tubes quickly where the change of contact points is reduced during analysis as

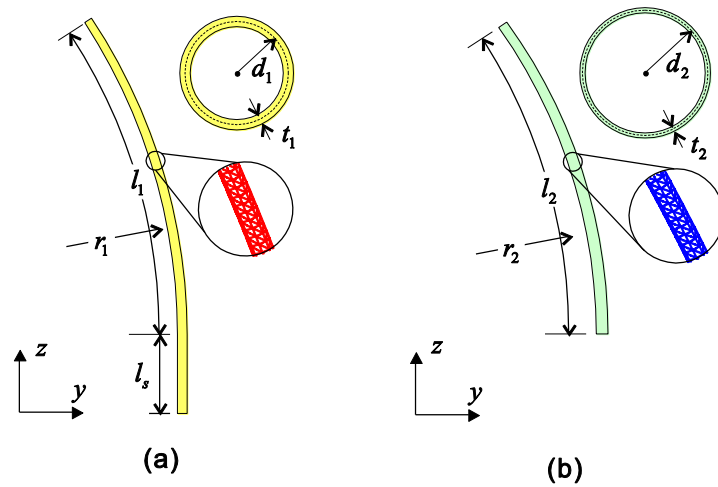


Fig. 3 Geometry and the finite element model of (a) the inner tube and (b) the outer tube

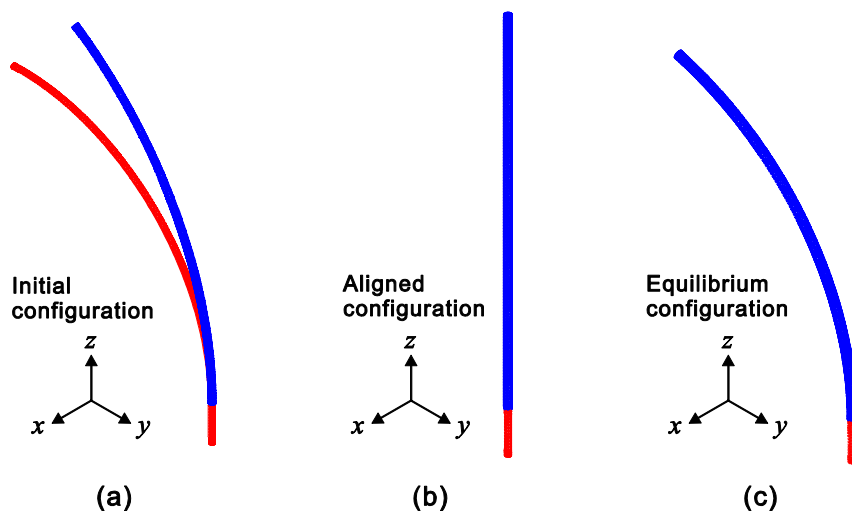


Fig. 4 Tube assembly procedure

described below.

Tube assembly begins with creating the finite element model for each tube individually. For two-tube robots, the inner and outer tubes that usually have different curvatures are constructed independently and discretized using the MITC shell elements (Fig. 3). In this initial configuration, the tubes overlap but do not interact with each other as contact conditions are not imposed yet (Fig. 4(a)). Unlike the outer tube, the inner tube has a straight region whose end is connected to a motor for actuation in a real robot system. While the tubes are made of biocompatible nitinol alloys that exhibit unique properties such as shape memory and superelasticity (Auricchio and Sacco 1999), isotropic linear elastic material model is used for the tubes because the robot operates in the range of linear elasticity.

Next, we apply the displacements to the tubes so that they become straight and concentric in the aligned configuration (Fig. 4(b)). During this process, the tubes can penetrate each other

because contact conditions are still inactive. Finally, we turn on the tube-tube contact condition and then release gradually the applied forces required to maintain the tubes straight in the aligned configuration until the tube assembly finds its bent, equilibrium configuration (Fig. 4(c)). Both tubes become stressed in this final configuration unless they have the same initial curvature. The proposed alignment-relaxation approach to assembling multiple tubes is significantly more reliable and efficient than the naive, plug-in approach.

3.2 Robot actuation

Once the finite element model for tube assembly is constructed, we perform nonlinear dynamic analysis to obtain the robot trajectories in response to actuation inputs. It is natural to adopt the implicit time integration method here because tube robots are manipulated slowly in practice. In the total Lagrangian framework, the incremental equilibrium equations to be solved for the robot dynamics are

$$\mathbf{M}^{t+\Delta t} \ddot{\mathbf{U}} + \mathbf{C}^{t+\Delta t} \dot{\mathbf{U}} + {}_0^t \mathbf{K} \Delta \mathbf{U} = {}^{t+\Delta t} \mathbf{R} - {}_0^t \mathbf{F} \quad (10)$$

where \mathbf{M} is the mass matrix, \mathbf{C} is the damping matrix, $\Delta \mathbf{U}$ is the incremental displacements from time t to time $t + \Delta t$, ${}^{t+\Delta t} \dot{\mathbf{U}}$ and ${}^{t+\Delta t} \ddot{\mathbf{U}}$ are the velocities and accelerations at time $t + \Delta t$, respectively, ${}^{t+\Delta t} \mathbf{R}$ represents the externally applied forces at time $t + \Delta t$, ${}_0^t \mathbf{F}$ is the internal forces at time t and ${}_0^t \mathbf{K}$ is the tangent stiffness matrix at time t .

To solve Eq. (10) accurately, the Bathe method is employed which is one of the recent implicit time integration schemes demonstrating its reliability and efficiency for the solution of various nonlinear problems in structural dynamics (Bathe and Baig 2005, Bathe 2007, Bathe and Noh 2012, Noh *et al.* 2013). In principle, this method divides the complete time step Δt into two sub-steps and uses the trapezoidal rule for the first sub-step and the 3-point Euler backward method for the second one. More specifically, the following approximations are used for the first sub-step

$${}^{t+\gamma\Delta t} \dot{\mathbf{U}} = \frac{2}{\gamma\Delta t} ({}^{t+\gamma\Delta t} \mathbf{U} - {}^t \mathbf{U}) - {}^t \dot{\mathbf{U}} \quad (11a)$$

$${}^{t+\gamma\Delta t} \ddot{\mathbf{U}} = \frac{4}{\gamma^2 \Delta t^2} ({}^{t+\gamma\Delta t} \mathbf{U} - {}^t \mathbf{U} - \dot{\mathbf{U}} \gamma \Delta t) - {}^t \ddot{\mathbf{U}} \quad (11b)$$

and for the second sub-step

$${}^{t+\Delta t} \dot{\mathbf{U}} = \frac{(1-\gamma)}{\gamma\Delta t} {}^t \dot{\mathbf{U}} - \frac{1}{(1-\gamma)\gamma\Delta t} {}^{t+\gamma\Delta t} \dot{\mathbf{U}} + \frac{(2-\gamma)}{(1-\gamma)\Delta t} {}^{t+\Delta t} \dot{\mathbf{U}} \quad (12a)$$

$${}^{t+\Delta t} \ddot{\mathbf{U}} = \frac{(1-\gamma)}{\gamma\Delta t} {}^t \ddot{\mathbf{U}} - \frac{1}{(1-\gamma)\gamma\Delta t} {}^{t+\gamma\Delta t} \ddot{\mathbf{U}} + \frac{(2-\gamma)}{(1-\gamma)\Delta t} {}^{t+\Delta t} \ddot{\mathbf{U}} \quad (12b)$$

where $t+\gamma\Delta t$ is a sub-step between t and $t+\Delta t$ with $\gamma \in (0,1)$ which is set to be 0.5 in this work. Substituting Eqs. (11)-(12) into Eq. (10) results in the following time-stepping equations

$$\hat{\mathbf{K}}_1 {}^{t+\gamma\Delta t} \mathbf{U} = \hat{\mathbf{R}}_1 \quad (13a)$$

$$\hat{\mathbf{K}}_2^{t+\Delta t} \mathbf{U} = \hat{\mathbf{R}}_2 \quad (13b)$$

where $\hat{\mathbf{K}}_1$ and $\hat{\mathbf{K}}_2$ are effective stiffness matrices, and $\hat{\mathbf{R}}_1$ and $\hat{\mathbf{R}}_2$ are effective nodal load vectors. More detailed descriptions about the method are well illustrated in Refs (Bathe and Baig 2005, Bathe 2007, Bathe and Noh 2012, Noh *et al.* 2013).

During this actuation process, it is important to apply proper contact conditions between the tubes efficiently. We assume frictionless contacts in our analysis, imposed using the constraint function method (Bathe and Bouzinov 1997), because it has been shown that frictions do not affect the robot trajectories (Lock and Dupont 2011). In order to capture the hysteretic behaviors of the robot observed experimentally, we include the damping force in contact as

$$\mathbf{F}_{damp} = C_N \dot{\mathbf{u}}_N + C_T \dot{\mathbf{u}}_T \quad (14)$$

where C_N and C_T are the damping coefficients in the normal and tangential directions, respectively, while $\dot{\mathbf{u}}_N$ and $\dot{\mathbf{u}}_T$ are the relative normal and tangential velocities, respectively, between the nodes in contact. In practice, isotropic damping ($C_N=C_T$) is used for dynamic analysis of the robot as explained in the next section.

4. Results

Here, we construct three two-tube continuum robots whose behaviors were tested and characterized experimentally (Dupont *et al.* 2010). The inner tube consists of the straight part whose length is $l_s=18$ mm and the curved part whose radius of curvature is ρ_1 while the outer tube has the curved part only whose radius of curvature is ρ_2 . The inner tube and the outer tube have the diameters of $d_1=2.19$ mm and $d_2=2.66$ mm, the thicknesses of $t_1=0.44$ mm and $t_2=0.22$ mm, and the arc lengths of $l_1=150$ mm and $l_2=150$ mm, respectively. Three robots simulated here differ only in curvatures of the inner and outer tubes (Table 1). The inner and outer tubes are discretized using 1,912 and 2,386 MITC6 shell elements, respectively, resulting in the finite element models with 51,984 DOFs in total. We use the linear elastic material properties of nitinol corresponding to Young's modulus of $E=48.87$ N/mm² and Poisson's ratio of $\nu=0.3$. Note that there may exist unpredictable variations of these properties in real robot systems due to heat treatment during annealing process for making pre-curved tubes.

To actuate the finite element robot model, we apply a clockwise or counterclockwise rotational input to the base of the inner tube that is actuated by a motor in a real system while fixing the base position of the outer tube. The relative twist angles at the distal end, $\alpha(L)$, are calculated as a function of the applied motor input, α_m , and compared with the experimental

Table 1 Specification of two-tube robots

Tube robot	Radius of Curvature (mm)	
	Outer tube	Inner tube
A	242	260
B	154	154
C	93	93

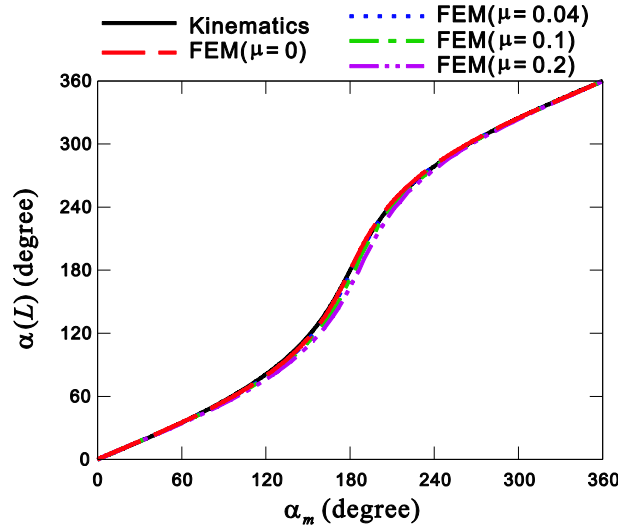


Fig. 5 Effect of frictions on the relative twisting angle curve of tube robot B

measurements. We also calculate them using the kinematic model by solving Eqs. (7)-(9) simultaneously for comparison. Since only curved parts of the tube are modeled in the kinematic approach, we calculate $\alpha(s)$ and $\dot{\alpha}(s)$ in the curved region first by applying rotational inputs at the end of the curved region of the inner tube near its base corresponding to the motor input related by

$$\alpha_m = \alpha(0) - \dot{\alpha}(0) \cdot L_{ext} \cdot \frac{G_1 J_1}{(G_1 J_1 + G_2 J_2)} \quad (15)$$

where $L_{ext}=l_s$ is the length of the extended part of the inner tube (Dupont *et al.* 2010).

First, we investigate the effect of contact parameters used to model tube-tube interactions. Finite element analysis with various friction coefficients (Fig. 5) verifies that the frictional force does not affect the robot trajectories as observed in analysis with the kinematic model (Lock and Dupont 2011). While the result for tube robot B is only given in Fig. 5, the same results are observed in the other tube robots as well. On the other hand, the damping force in contact influences the dynamics of the tube robot significantly, particularly its hysteretic behavior. In general, different damping coefficients need to be defined in the normal and tangential directions, which makes it difficult to identify proper values in practice. However, similar to frictions, we can choose any set of values for these coefficients, C_N and C_T in Eq. (14), as long as the total amount of contact damping remains the same because the resultant force governs the robot behavior not its components (Fig. 6). While the result for tube robot B is only given in Fig. 6, the same results are observed in the other tube robots as well. Hence, for simplicity, we assume the isotropic damping, $C_N=C_T=C_{cont}$, in this study.

It is important to note that our finite element analysis reproduces the kinematic modeling solutions without hysteresis when the effect of contact damping is not included. There exist slight differences between these solutions, which might be attributable to certain factors that are not considered in the kinematic model but modeled in the finite element analysis including the gap between the tubes and the extension and shear of the tubes. As the damping coefficient increases,

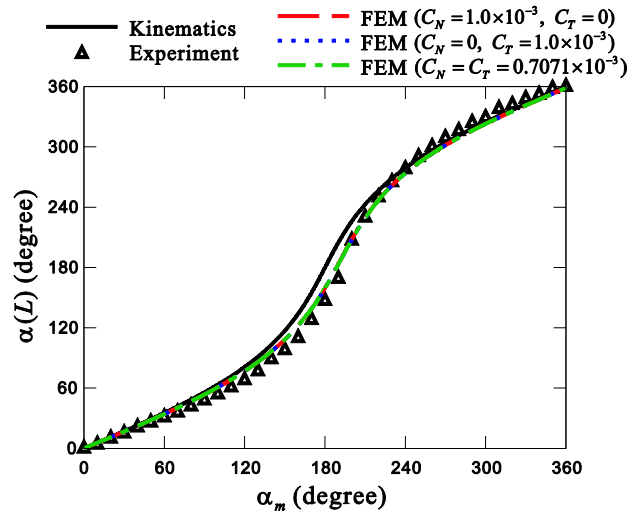


Fig. 6 Effect of contact damping forces on the relative twisting angle curve of tube robot C

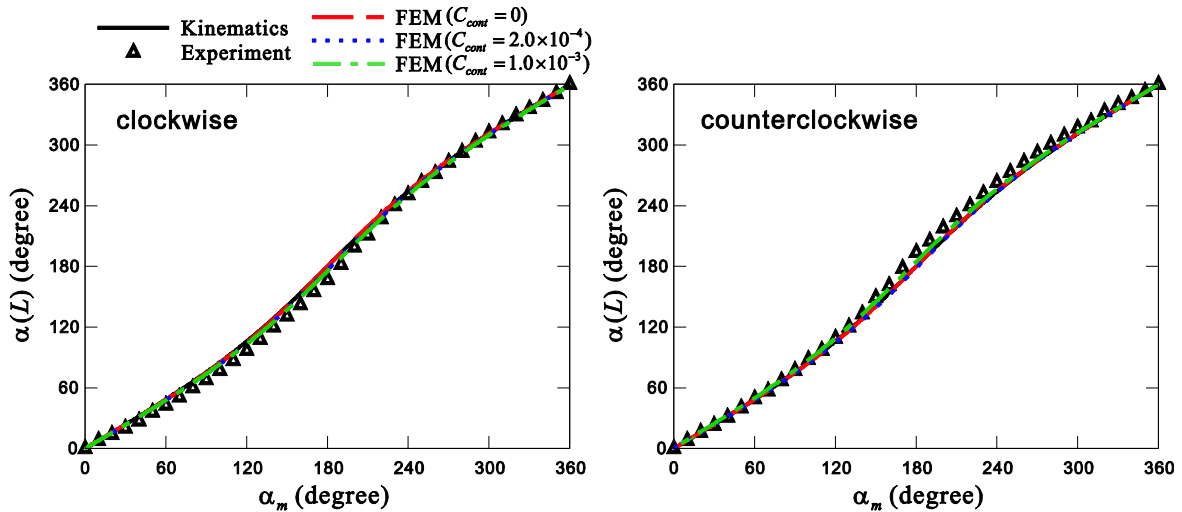


Fig. 7 Relative twisting angle curve of tube robot A

however, the finite element solutions become more deviated from the kinematic solutions forming a complete hysteresis loop.

Tube robot A consists of two low-curvature tubes whose radius of curvature when assembled is 250 mm. Its relative twist angle curve (Fig. 7) is similar to that of the concentric straight tubes where the relative twist angle at the distal end coincides simply with the applied motor input. In this case, both kinematic and finite element models reproduce experimentally obtained results fairly well except that the kinematic model cannot capture the hysteretic behavior. This incapability of the kinematic model deteriorates its solution accuracy more when analyzing more highly curved tube robots.

The relative twist angle curves of tube robot B whose radius of curvature is 154 mm clearly

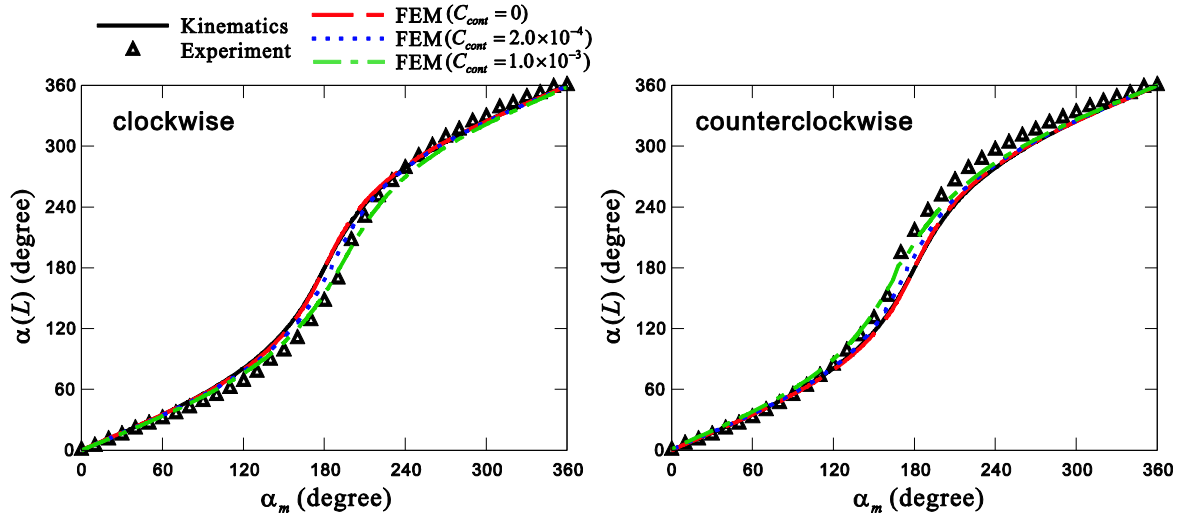


Fig. 8 Relative twisting angle curve of tube robot B

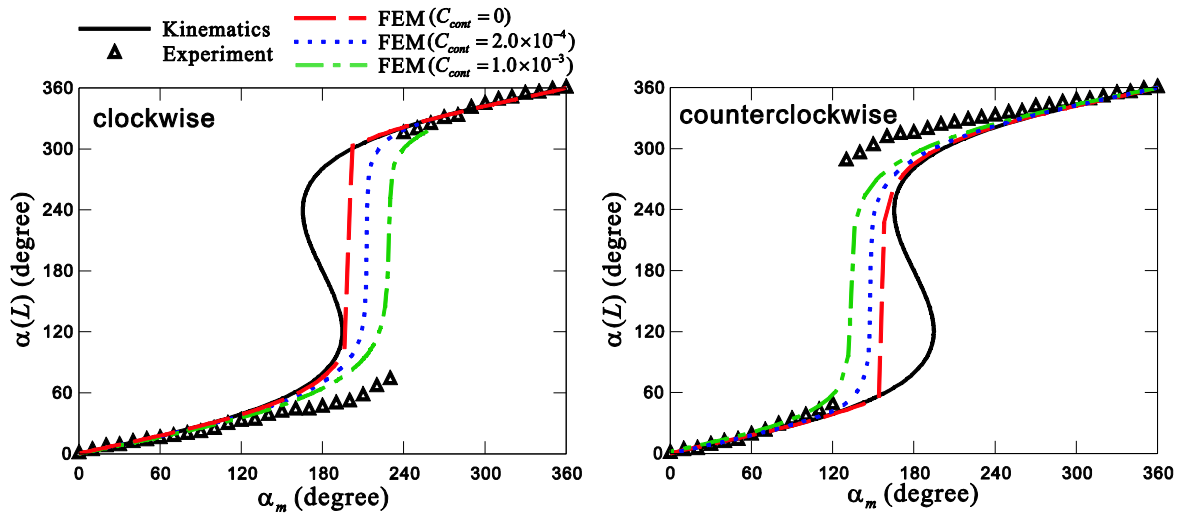


Fig. 9 Relative twisting angle curve of tube robot C

show the discrepancy between the experimental measurements and the kinematic solutions that amounts to 37.4 degree at maximum (Fig. 8). In contrast, the proposed finite element model not only provides the solutions that are much closer to the experimental measurement but also reproduces the hysteretic behavior of the robot successfully.

Tube robot C consisting of the tubes with the smallest radius of curvature suffers from the snapping problem. It is important to predict not only whether but also when this snapping phenomenon occurs accurately because this would be quite perilous in robot-aided surgeries. Experiments reveal that the snapping occurs when $\alpha_m=230^\circ$ and $\alpha_m=120^\circ$ for clockwise and counterclockwise inputs, respectively (Fig. 9). The kinematic model predicts, however, that the snapping takes place much earlier than experiments ($\alpha_m=194^\circ$ and $\alpha_m=165^\circ$ for clockwise and

counterclockwise inputs, respectively). The motor inputs when the snapping occur predicted using the finite element model are quite close to the experimentally observed values ($\alpha_m=227^\circ$ and $\alpha_m=132^\circ$ for clockwise and counterclockwise inputs, respectively). Note that the finite element solutions converge to the kinematic solutions when contact damping is not considered. Nevertheless, there exist a marked discrepancy between the relative twist angle curves near the snapping point, which might be due to unmodeled features including the slipping of the tube with respect to the attached motor and the phase transition of tube properties at local positions during annealing process.

5. Conclusions

We present the finite element modeling approach to investigating the dynamics of concentric-tube continuum robots. Analysis consists of two steps: (1) tube assembly step where the assembled configuration of the precurved tubes is calculated and (2) robot actuation step where the actuating inputs are applied to compute the tube trajectories. MITC shell elements are employed to model the tubes and their dynamic responses are predicted implicitly using the Bathe time integration scheme. Damping forces between the tubes in contact are included to capture the hysteretic behavior of the robot that is experimentally observed. Results for three two-tube robots are shown to demonstrate the performance of the proposed method. Our finite element model provides more accurate solutions than the more commonly used kinematic model particularly for the hysteresis in the relative twist angle curves and the actuating input when the snapping occurs.

Acknowledgments

This work was supported by the Center for Advanced Meta-Materials (CAMM) funded by the Ministry of Science, ICT & Future Planning as Global Frontier project (CAMM-2014M3A6B3063711). This work was also supported by the National Research Foundation of Korea (NRF) Grant funded by the Ministry of Science, ICT & Future Planning for convergent research in sport scientification (NRF-2014M3C1B1033983). Changyeob Baek was supported by SNU Undergraduate Research Program.

References

- ADINA R&D (2013), *ADINA Theory and Modeling Guide*, ADINA R&D, Watertown, MA.
- Auricchio, F. and Sacco, E. (1999), "A temperature-depedent beam for shape-memory alloys: constitutive modelling, finite-element implementation and numerical simulations", *Comput. Struct.*, **174**, 171-190.
- Bathe, K.J. and Bouzinov, P. (1997), "On the constraint function method for contact problems", *Comput. Struct.*, **64**, 1069-1085.
- Bathe, K.J. and Baig, M.M.I. (2005), "On a composite implicit time integration procedure for nonlinear dynamics", *Comput. Struct.*, **31-32**, 2513-2524.
- Bathe, K.J. (2007), "Conserving energy and momentum in nonlinear dynamics: a simple implicit time integration scheme", *Comput. Struct.*, **85**, 437-445.
- Bathe, K.J. and Noh, G. (2012), "Insight into an implicit time integration scheme for structural dynamics", *Comput. Struct.*, **98-99**, 1-6.

- Burgner, J., Swaney, P.J., Rucker, D.C., Gilbert, H.B., Nill, S.T., Russell, P.T., Weaver, K.D. and Webster, R.J. (2011), "A bimanual teleoperated system for endonasal skull base surgery", *Proc. IEEE/RSJ Int. Conf. Intell. Robot. Syst.*, 2517-2523.
- Burgner, J., Swaney, P.J., Lathrop, R.A., Weaver, K.D. and Webster, R.J. (2013), "Debulking from within a robotic steerable cannula for intracerebral hemorrhage evacuation", *IEEE Tran. Biomed. Eng.*, **60**, 2567-2575.
- Burgner, J., Rucker, D., Gilbert, H., Swaney, P., Russel, P., Weaver, K. and Webster, R. (2014), "A telerobotic system for transnasal surgery", *IEEE/ASME Tran. Mech.*, **19**, 996-1006.
- Dupont, P.E., Lock, J. and Bulter, E. (2009), "Torsional kinematic model for concentric tube robots", *Proc. IEEE Int. Conf. Robot. Autom., Kobe, Japan*, 3851-3858.
- Dupont, P.E., Lock, J., Itkowitz, B. and Bulter, E. (2010), "Design and control of concentric tube robots", *IEEE Tran. Robot.*, **26**, 209-225.
- Gilardi, G. and Sharf, I. (2002), "Literature survey of contact dynamics modeling", *J. Mech. Mach. Theory*, **37**, 1213-1239.
- Kim, D.N. and Bathe, K.J. (2008), "A 4-node 3D-shell element to model shell surface tractions and incompressible behavior", *Comput. Struct.*, **86**, 2027-2041.
- Kim, D.N. and Bathe, K.J. (2009), "A triangular six-node shell element", *Comput. Struct.*, **87**, 1451-1460.
- Lock, J. and Dupont, P.E. (2011), "Friction modeling in concentric tube robots", *Proc. IEEE Int. Conf. Robot. Autom.*, 1139-1146.
- Lee, P.S. and Bathe, K.J. (2004), "Development of MITC isotropic triangular shell finite elements", *Comput. Struct.*, **82**, 945-962.
- Lee, Y.G., Yoon, K. and Lee, P.S. (2012), "Improving the MITC3 shell finite element by using the Hellinger-Reissner principle", *Comput. Struct.*, **110-111**, 93-106.
- Noh, G., Ham, S. and Bathe, K.J. (2013), "Performance of an implicit time integration scheme in the analysis of wave propagations", *Comput. Struct.*, **123**, 93-105.
- Rucker, D.C., Webster, R.J., Chirikjian, G.S. and Cowan, N.J. (2010), "Equilibrium conformations of concentric-tube continuum robots", *Int. J. Robot. Res.*, **29**, 1263-1280.
- Sears, P. and Dupont, P. (2006), "A steerable needle technology using curved concentric tubes", in *Proc. IEEE/RSJ Int. Conf. Intell. Robot. Syst.*, 2850-2856.
- Webster, R.J., Okamura, A.M. and Cowan, N.J. (2006), "Toward active cannulas: Miniature snake-like surgical robots", *Proc. IEEE/RSJ Int. Conf. Intell. Robot. Syst.*, 2857-2863.
- Webster, R.J., Romano, J.M. and Cowan, N.J. (2009), "Mechanics of precurved-tube continuum robots", *IEEE Tran. Robot.*, **25**, 67-78.